Rock and Soil Mechanics

Volume 41 | Issue 1 Article 4

9-23-2020

Research on direct shear behaviour and fracture patterns of 3D-printed complex jointed rock models

Pei-tao WANG
Beijing Key Laboratory of Urban Underground Space Engineering, University of Science and Technology Beijing, Beijing 100083, China

Zheng-jun HUANG
Key Laboratory of Ministry of Education for Efficient Mining and Safety of Metal Mine, University of Science and Technology Beijing, Beijing 100083, China

Fen-hua REN
Key Laboratory of Ministry of Education for Efficient Mining and Safety of Metal Mine, University of Science and Technology Beijing, Beijing 100083, China

Liang ZHANG
Key Laboratory of Ministry of Education for Efficient Mining and Safety of Metal Mine, University of Science and Technology Beijing, Beijing 100083, China

See next page for additional authors

Custom Citation

WANG Pei-tao, HUANG Zheng-jun, REN Fen-hua, ZHANG Liang, CAI Mei-feng, . Research on direct shear behaviour and fracture patterns of 3D-printed complex jointed rock models[J]. Rock and Soil Mechanics, 2020, 41(1): 46-56.

Research on direct shear behaviour and fracture patterns of 3D-printed complex jointed rock models

Authors

Pei-tao WANG, Zheng-jun HUANG, Fen-hua REN, Liang ZHANG, and Mei-feng CAI

Rock and Soil Mechanics 2020 41(1): 46−56 ISSN 1000−7598
https: //doi.org/10.16285/j.rsm.2018.7247 rocksoilmech.researchcommons.org/journal

Research on direct shear behaviour and fracture patterns of 3D-printed complex jointed rock models

WANG Pei-tao[1, 2, 3], HUANG Zheng-jun[1], REN Fen-hua[1], ZHANG Liang[1], CAI Mei-feng[1]

1. Key Laboratory of Ministry of Education for Efficient Mining and Safety of Metal Mine, University of Science and Technology Beijing, Beijing 100083, China
2. Department of Civil, Environmental and Geo-engineering, University of Minnesota, Minneapolis, USA
3. Beijing Key Laboratory of Urban Underground Space Engineering, University of Science and Technology Beijing, Beijing 100083, China

Abstract: Geometry and mechanical characteristics of joints are key factors affecting the shear behaviors and fracture patterns of jointed rock mass. Using 3D printing technique, experimental jointed rock specimens containing rough joints with varied joint roughness coefficient (JRC), different types of geometrical joints, and fractrues network were established respectively. Then direct shear tests were conducted on the jointed rock models to study the shear strength and failure patterns. The results show that the values of shear strength of jointed rock models fluctuate greatly with varied JRC curves. The peak shear displacement decreases with increasing amplitude of fluctuation. The lowest and highest values of shear strength are found in plane and rectangular joints, respectively. Moreover, the value of shear strength of sinusoidal type is found similar to that of triangular type. The shear strength of the 3D-printed fractured rock specimens are apparently lower than that of the intact rock specimens. When considering joint roughness, the peak shear stresses of rough discrete fractures network (RDFN) models are higher than those of the discrete fractures network (DFN) models. The solid rock specimens exhibit typical brittle shear failure. The fracture patterns of DFN model and RDFN model are relatively complex and the main shear fractures are found along the shear direction. Meanwhile, certain intersection points between joints and certain surfaces have significant influence over the shear failures. The present work provides references for the application of 3D printing technique in studying the shear behaviors of fractured rock masses.

Keywords: jointed rock mass; 3D printing; direct shear test; fractures patterns; experimental study

1 Introduction

Shear property of jointed rock mass is one of the most important factors which greatly influence the stability analysis in geotechnical engineering. It has been widely investigated in rock engineering[1-3], especially slope engineering, in which the shear property directly affects the rock slide. There are plenty of natural joints which are complex and randomly distributed as Fig.1 shows. The distribution and mechanical properties of joints will control the initiation and propagation of fractures in the jointed rock mass. Thus it is vital to study the joints characterization techniques and the corresponding influence of complex joints on the shear behaviours of jointed rock mass, which will supply scientific evidence for the stability of rock engineering.

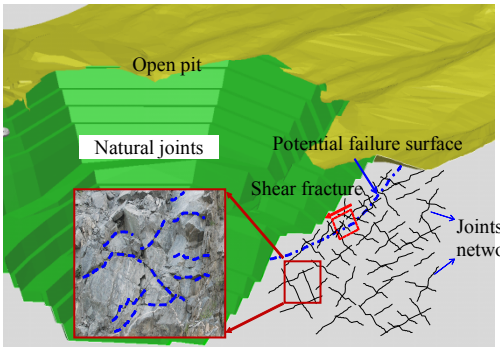

Fig.1 Schematic diagram of structurally controlled landslide of jointed rock slope

Many researchers have conducted experimental tests on the shear behaviours of joints. According to Goodman[4], the nonlinear deformation of joints should be attributed to the existence and failure of the micro-convexes, which outlined the microscopic failure mechanism of jointed rock mass. Barton[5] suggested a joint roughness coefficient, JRC, to represent the complex joints based on numerous experimental tests on rock mass discontinuities. The shear strength of the joints relates to both the normal stress and the JRC value. Barton then proposed three JRC curves (5, 10, and 20) to represent the joints. Later, Barton et al. [6] proposed ten JRC curves according to 136 rock specimens under shear test. The ten curves were then used as

Received: 11 November 2018 Revised: 28 April 2019
This work is supported by the National Key R&D Program of China (2018YFE0101100), the National Natural Science Foundation of China (51604017, 51774022) and the Fundamental Research Funds for the Central Universities (FRF-TP-18-026A2).
First author: WANG Pei-tao, male, born in 1987, associate Professor, Research interest: stability and anisotropy of jointed rock mass. E-mail: wangpeitao@ustb.edu.cn.

suggested methods for the quantitative description of discontinuities in rock masses by ISRM (International Society for Rock Mechanics) [7]. This work plays a significant role in guiding the quantitative characterization and analysis of shear properties for jointed rock masses. Bardis et al.[8] established a model for estimating the shear strength of rock joints based on numerous shear tests, and the correlation between the roughness and shear strength of rock joints was rectified and quantified.

Many research results[9-13] have shown that the joint geometry significantly affects the shear failure mode and shear strength of jointed rock when direct shearing is performed along a single joint surface. By measuring the roughness of the natural structure surface, Singh et al. [14-15] used the JRC to characterize the roughness of the joints and studied the effect of JRC on shear strength under different normal stress conditions. Zhao et al.[16] studied the roughness reduction along the joint surface under shearing, and conducted a numerical study on the influence mechanism of solute flow. It was found that the joint surface geometry changed significantly after shear failure according to the study. Niktabar et al. [17] carried out cyclic shear tests on rocks with rough joints and considered the geometry of regular and irregular inclination angles, respectively. It was found that the shear strength of the specimens increased with increasing inclination angle and normal stress at first shear cycle. Cheng et al. [18] studied the size effect of rock shear strength under shear conditions and found that there were some differences in shear strength under different size conditions. Tian et al.[19] established a single triangular undulating joint model using similar filling materials under different filling conditions. The test results show that the undulating position of the joint step is prone to fracture during shearing, which indicates the property of filling materials and the joints geometry are key influencers when analyzing shear strength of jointed rocks. Zhou et al.[20] studied the shear behaviours of toothed surfaces with different amplitudes, and found that the amplitude of tooth had a great effect on shear sliding and shear characteristics. The corresponding shear strength analysis model was also derived. These research results fully show that the roughness of joints significantly impacts the macro mechanical behaviors of jointed rock masses, such as seepage characteristics, uniaxial compression mechanical properties. It is also one of the principal intrinsic factors which determines the shear strength of rock masses.

Due to the limitation of the current modeling methods of complex joint models and physical experimental modeling conditions, relatively few studies on the shear mechanical properties of joints with consideration of joints roughness have been made. The impact of rough joints on the shear behaviours of jointed rock masses and their corresponding failure mechanisms still need further investigation. With the development of the 3D printing (3DP) technology, modeling of complex structures has gradually become possible. 3DP technology has the advantages of applying in “any material, any part, any number, any location, and any field[21]”. Thus attentions have been paid by many researchers in rock mechanics and rock engineering[22-27]. Xie et al.[28] applied 3DP technology in modeling the rock specimens with fractures inside. Ju et al. [29] analyzed mechanical behaviors, such as stress evolution, crack propagation and instability. This research is of great significance for promoting the research methods for deep rock mechanics. Xiong et al. [30] carried out a series of direct shear tests on joints using 3D printing technology. The test results showed that the properties of samples were consistent with each other and the feasibility of 3DP technology in rock mechanics is verified. Tian et al.[31] used 3DP technology to produce rock samples within internal structures identical to sandstone samples. The test results show that the strength and fracture modes are close to those of the natural sandstones. Wang et al. [32] produced a series of fractures network models using 3DP technology, and then compared the effect of geometric roughness on the uniaxial compression properties of the jointed models. The study shows the feasibility of 3DP in the study of complex jointed rock masses in laboratory experiments analysis. Zhu et al. [33] used the CT scanning and 3DP technology to print some porous rocks made of resin materials. According to the result, the uniaxial compressive strength (UCS) and dynamic Brazilian splitting strength were close to volcanic rocks, which had a good agreement with the numerical simulations. The study provides a useful reference for 3DP technology and laboratory test research of rock materials with complex pores and fractures, as well as promotes the popularization and application of 3DP technology in geotechnical engineering. Song et al. [34] used 3DP technology to produce a tunnel model based on polyacetic acid (PLA) and gypsum material, and carried out laboratory experiments on tunnel stability. The results showed that the mechanical properties of the 3DP tunnel model were basically stable, which provided a reference for the application of 3DP technology in the tunnel engineering. Kong et al. [35-36] established some gypsum rock samples using 3DP technology. Among the gypsum samples, different pore distributions and morphologies were considered and the pore distribution was obtained by CT scanning. The results show that 3D-printed samples can effectively reflect the pore distribution of the digital model. However, Kong et al.[35] also proposed that 3DP samples have layered structures, which induces significant

transverse isotropic characteristics. The influence of the structures cannot be ignored in the study of rock-like mechanical properties. Zhou et al.[37] used 3D scanning and engraving techniques to prepare rock structural surface with different roughness and discussed the shear anisotropy characteristics of the structural surface, which provided a useful method for preparing structural surfaces and studying mechanical properties. All these research results show that 3DP technology provides an effective way for physical modeling of complex rock mass structures. By physically reconstructing complex structures, experimental models suitable for indoor simulations can be established, thus providing effective methods and approaches for experimental study on mechanical behaviors of complex fractured rock masses.

In this study, direct shear tests were conducted on several printed rock samples based on 3DP technology. Ten Barton rough joint curves were established first by 3D digital model, 3D solid printing and model preparation, to investigate the effect of different JRC curves on shear strength. And then, four different geometries (sine type, rectangle type, triangle type, and plane type) and different PLA materials were prepared. The influence of joint geometry on shear characteristics was discussed together with the shear properties of PLA materials. Finally, the linear discrete fractures network (DFN) model and the rough discrete fractures network (RDFN) model were established respectively. The shear behavior of fractured rock mass models was studied by physical experiments. The mechanical behaviours of different jointed models under direct shear conditions were analyzed and the influence of geometric roughness of joints on the shear mechanical properties was discussed. The research will provide a useful reference for the study of shear behaviours of jointed rock masses by 3DP technology.

2 3D printing models

3D printer, named XYZ Printing DaVinci 3.0 (as shown in Fig.2(a)), was used to model the joint samples. The nozzle diameter of the 3DP system is 0.4 mm with printing accuracy of 0.1 mm. The maximum model size is 200 mm × 200 mm × 190 mm (Length×width×height). The 3DP printing method used in this paper is fused deposition modeling (FDM). PLA polymer plastic is used as the printing material. The 3DP sample is produced by layering and fusion stacking. For this test, the printing layer thickness is 0.3 mm. The filling ratio is an important parameter for the 3D printing. This index represents the proportion of internal filling when printing a 3D solid model, which is directly related to the porosity of the model. The higher the printing filling ratio, the lower the porosity of the model will be. When the filling ratio is set to be 0%, only the empty shell is printed. When the filling rate is 100%, the printing material will be filled completely.

There are two filling approaches in the 3DP system, namely intertwining filling and honeycomb filling, as shown in Figs.2(b) and 2(c). The printing efficiency of different filling methods are also different, with all models are chosen to be intertwining filling here.

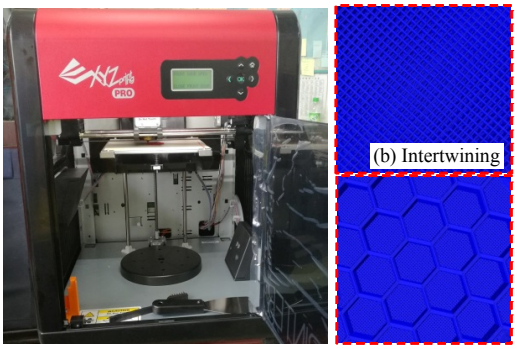

(a) XYZ Printing DaVinci 3D printer (c) Honeycomb filling

Fig.2 XYZ Printing DaVinci 3D printing system

The steps of establishing the Barton's JRC joints model are as follows:

(1) Selecting the Barton joint curve, carrying out the 2D reconstruction of the digital joint image in AutoCAD by recognizing and widening the line image. Considering the effective accuracy of the 3D printer, the stretch width is 1.5 mm.

(2) Using the "Region" command to generate the fissure regions, and then using the "Extrude" command to stretch these fissure regions to a height of 20 mm and obtain a three-dimensional JRC curve model.

(3) Exporting the "* .STL" files of each model by AutoCAD and importing into XYZware Pro printing software. Setting the relevant 3D printing parameters to prepare a Barton' JRC joints model.

Fig.3(a) shows the 10 JRC curves proposed by Barton et al[6]. A three-dimensional model of different JRC digital joint surfaces is established (Fig.3(b)). In this work, the length, thickness and height of the model are 50 mm, 1.5 mm and 20 mm, respectively. It should be noted that the thinner the printed joint model is, the more detailed the joint traces will be. Due to the accuracy limitation of the 3D printer, the thickness of 1.5 mm was chosen in this printing after many tests. With the development of 3D printer, the thickness of the joint model should be minimized. Different JRC surfaces obtained by 3D printing are shown in Fig.3(c). To ensure the efficiency, the filling ratio was 20% in the model, and the filling thickness was

approximately 0.3 mm. Because the model is created by the FDM method, the stacking boundary of each layer is significant. The printing surface undulations were consistent with the two-dimensional joint digital models.

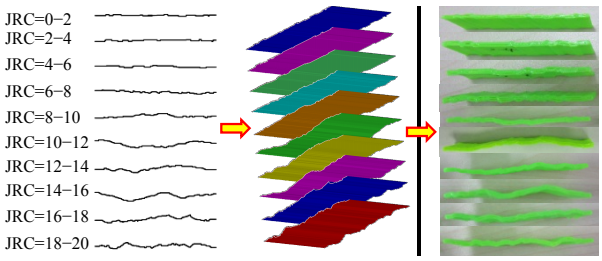

(a) Barton's JRC curves (b) Extension (c) 3D-printed models

Fig.3 Barton proposed curves with varied JRC values and corresponding 3D models

The shearing model and the settlement of the joint are shown in Fig.4. The JRC joint model was placed at the center of the model. The shear load was applied along the joint surface, and the load and displacement were monitored during the shear process to study the influence of different joint fluctuations on shear strength (Fig.4(a)). Since the length of the model was 50 mm, a printed PLA square box with size of 50 mm×50 mm× 20 mm was modeled. The joint was placed in the center of the test piece, and remains after curing completes, as shown in Fig.4(b). The sulphoaluminate fast hardening cement was used to model the harder rock material and cured in 20 ℃ water for 72 h. The jointed rock model is shown in Fig.4(c).

(a) Settlement of the model (b) Cemented model (c) Jointed specimen

Fig.4 Jointed rock specimen in experimental test

3 Experimental tests

3.1 Experimental system

The BC-100D rock shear system (Fig.5(a)) in the University of Science and Technology Beijing was used in this test. The maximum shear load of this machine is 100 kN and the maximum normal load is 50 kN. The MaxTest-Y2H direct shear controlling system was used to monitor and control the load and displacement. The load and displacement monitoring accuracy are 0.001 kN and 0.001 mm, respectively. This test only examines the peak shear strength of the material, so the direct shear test was conducted under normal stress of 0 MPa. The loading method adopted displacement control method and the shear rate was 0.3 mm/min. The shearing was performed until the specimen failed. Fig.5(b) is the shearing system and the settlement of the specimen. It should be noted that because the size of test model is unconventional, corresponding mold need to be processed to analyze the shear behaviours of different sizes. As shown in Fig.5(b), the shearing fixing mold fixes the specimen to prevent shear deflection of the specimen during the shearing process. Certain steel plates were placed in the mold to ensure that the shear load acts along the center of the specimens.

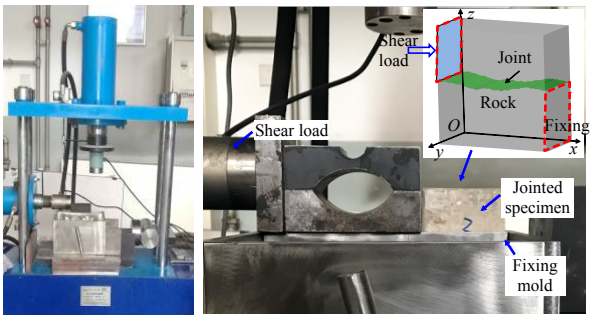

(a) BC-100D shearing machine (b) Shearing system

Fig.5 Schematic diagram of direct shear test system in laboratory test

3.2 Shear property of PLA material

To investigate the shear strength of PLA material, several PLA specimens with different filling ratio were prepared, as shown in Fig.6(a). Specimens with five filling ratios of 0%, 25%, 50%, 75% and 100% were prepared. All the samples were 30 mm×30 mm×20 mm in size with thickness of 0.3 mm. Fig.6(b) shows the shear results of the PLA models with filling ratios of 0%, 25%, 50%, 75% and 100%, respectively. Since the PLA specimen was made of plastic material, no macroscopic failure surface occurred during the shear process. Relatively large plastic deformation occurred and the residual shear strength was relatively stable during the shear progress (as shown in Fig.7). According to the shear failure results of PLA specimens under different filling rates, the square specimens exhibited high plastic deformation at different filling ratios, and no significant shear fracture was observed.

Fig.7(a) shows the shear stress-displacement curves of PLA specimens under different filling ratios. It is shown that PLA (polylactic acid) material exhibits significant plastic characteristics. At the pre-peak stage, the shear modulus of the elastic stage gradually increases as the filling ratio increases.

When the filling ratio is less than 100%, the residual shear strength of each specimen is close to the peak shear strength. As the filling ratio increases the residual shear strength also gradually increases. When the specimen is fully filled (filling ratio of 100%), the shear strength reaches 22.63 MPa. The shear stress in the residual stage shows a sudden drop phenomenon. Fig.7(b) shows the peak shear strength of the test specimens under different PLA filling ratios. The shear strength of PLA material increases with increasing filling ratio. The peak shear strength of PLA materials with a filling ratio of 0% is 1.42 MPa, which can be regarded as the shear strength of PLA joints.

(a) Before shear test

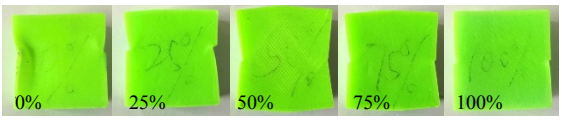

(b) After shear test

Fig.6 PLA model and failure patterns of specimens with varied filling rates

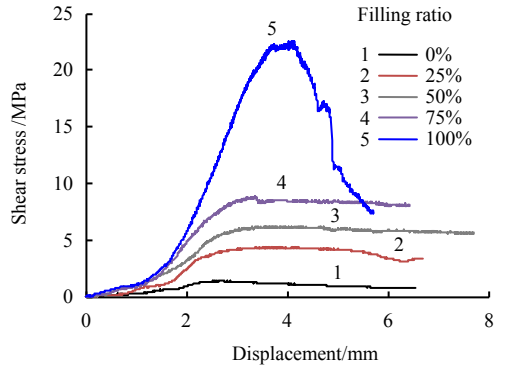

(a) Shear stress-displacement curves

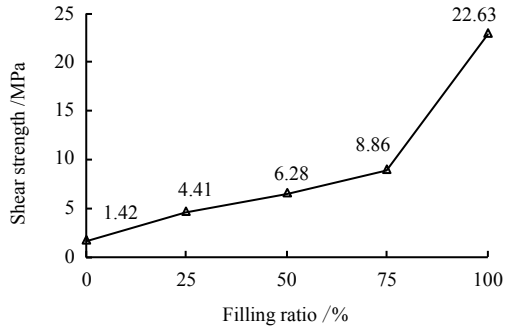

(b) Shear strength with varied filling ratio

Fig.7 Shear characteristics of PLA materials with varied filling rates

3.3 Shear property of rough joint model

The JRC joint models were placed in the center of the specimen and the shear direction was along the joint surface. In this shear test, the shear rate was set to be 0.5 mm/min until failure. The shear load and displacement were recorded and images were captured during the shear process.

The shear stress- displacement curves of joint models with different JRC models are shown in Fig.8 and the results are listed in Table 1. The results showed that there are significant differences in the shear characteristics of specimens under different JRC conditions. The shear stress fluctuates greatly as the shear displacement increases, indicating that the rock undergoes multiple contact-cut-recontact processes along the shear direction. Each joint specimen shows a distinct brittle shear failure mode. The specimens have relatively high shear strength under JRC of 2-4 and 12-14. Each specimen has certain residual shear strength in the post-peak shear stage.

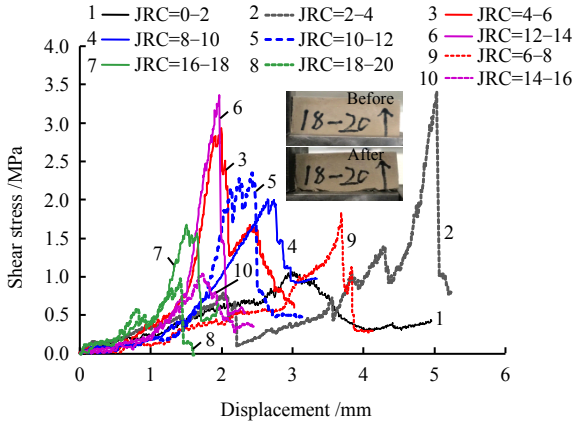

Fig.8 Shear stress-displacement curves of varied JRC rock specimens

Table 1 Shear behaviours of varied Barton rough joints

JRC	Shear strength /MPa	Peak shear displacement /mm	JRC	Shear strength /MPa	Peak shear displacement /mm
0-2	1.06	2.99	10-12	2.35	2.42
2-4	3.41	5.03	12-14	3.38	1.97
4-6	2.94	1.99	14-16	1.04	1.73
6-8	1.84	3.69	16-18	1.68	1.50
8-10	2.01	2.65	18-20	0.97	1.42

The fluctuation amplitude of the joint trace is directly related to the shear resistance property. The fluctuation amplitude of varied JRC curves is shown in Fig.9. It is observed that the amplitude generally increases with the increase of the JRC value. The amplitude of the fluctuation is relatively large for JRC values at 10-12 and 14-16. After 14-16, the amplitude of the joint fluctuation decreases as the JRC increases. Comparing the fluctuation amplitude and the peak shear strength, the magnitude of joint model fluctuation has a certain correlation with the peak shear strength. Changes in amplitude

fluctuations also correspond to significant changes in peak shear strength. Specimen with JRC of 8-10 has the highest peak shear strength while JRC of 18-20 is the lowest. It should be noted that the peak shear strength of specimens under different JRC conditions does not increase with the increase of JRC values. This is because the direct shear test does not consider the influence of normal stress in this test. Therefore, the peak shear strength mainly reflects the ability of sample to resist initial shear fracture. Fig.9(b) shows the correspondence between the peak shear displacement and the amplitude of fluctuation. It is found that the higher the fluctuation amplitude , the lower the peak shear displacement.

Fig.10(a) shows the shear failure modes of jointed specimens under different JRC conditions. According to the results, the shear failure modes of the model under different JRC situations show significant differences. Shear failure occurs basically along the joint surface, and crack initiation also occurs near the joint surface in some specimens, such as JRC of 2-4 and 6-8. Comparing with the shear failure mode of the solid specimen in Fig.10(b), the shear failure of the solid specimen shows a typical shear brittle failure mode, manifesting as a significant single shear crack. The shear failure mode is much more complicated for the jointed models. In addition to the main shear cracks, there are also a large number of cracks at the end of the shear boundary. There are some small-scale expanding cracks near the principal failure plane, indicating that the specimen undergoes multiple shear failure during the shear process, which is consistent with the shear stress fluctuation characteristics as shown in Fig.8.

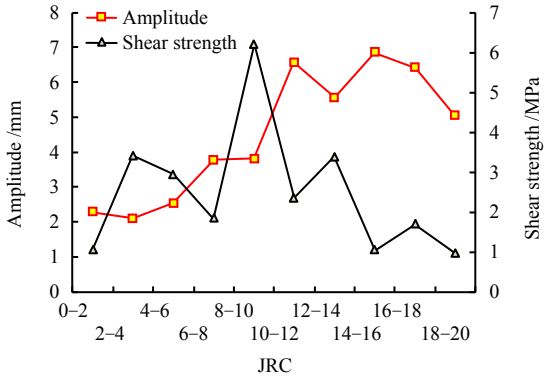

(a) Comparison of shear strength with amplitude

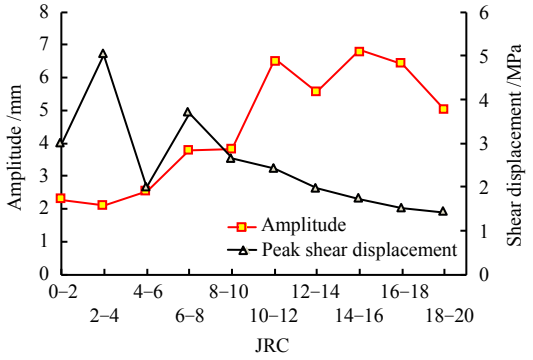

(b) Comparison of shear displacement with amplitude

Fig.9 Comparison of peak shear strength and fluctuation amplitude under different JRC conditions

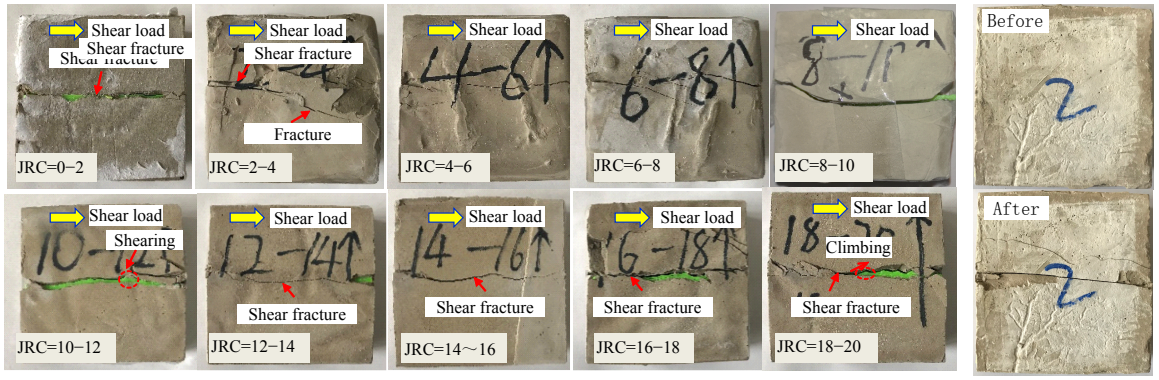

(a) Fracture patterns of specimens within joints of varied JRC (b) Fracture pattern of intact cement specimen

Fig.10 Shear failure patterns of jointed rock specimens of varied JRC values

4 Shear properties of specimens with complex joints networks

4.1 Fracture patterns of specimens with one rough joint

The shear characteristics of different Barton JRC joint models were discussed in the previous section. The results show that rough joint fluctuations have a significant effect on the shear behaviours. Joint surfaces generally have complex geometric distributions in natural rock masses. As Fig.11 shows, there are different geometric distributions such as arcs (Fig.11(a)), triangles (Fig.11(b)), and rectangles (Fig.11(c)). Different geometric trace shapes, especially different undulation

angles and amplitudes directly impact on the shear fractures of rocks. Thus the influence of different single joint geometrical undulations on the shear behavoiurs of jointed rocks needs to be studied.

In this section, four geometrical models of sine type, triangle type, planar type and rectangle type are established (Fig.12(a)), and the corresponding shear behaviours are tested. Fig.12(b) shows the 3D printed models of varied joints types. The model size is 60 mm×60 mm×20 mm, with fluctuation amplitude of the joint model as 20 mm and joint trace thickness of 0.3 mm.

(a) Arc type joint (b) Triangle type joint (c) Rectangle type joint

Fig.11 Complex joint morphologies of natural rock masses

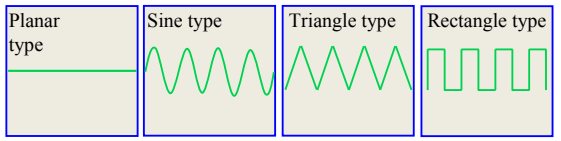

(a) Different geometric joints

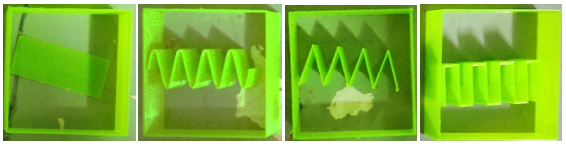

(b) 3D printed models

Fig.12 Joint models of varied geometries using 3D printing technique

Figs.13 and 14 show the shear stress- displacement curves and shear failure modes, respectively. To analyze the feasibility of 3D printed models, the results of each set of models (each set contains 3 samples) are shown in Fig.13. The shear strengths of jointed models with different geometric shapes are significantly different. According to the test, the planar shape has the lowest shear strength, while rectangular shape has the highest shear strength. The shear capacity of the sine and triangular specimens are close. For the same type of geometric model, although the shear stress-displacement curve in the pre-peak stage is different, the overall shape and trend are close. The result shows that it is feasible to conduct repeated shear mechanical test based on 3D printed specimens.

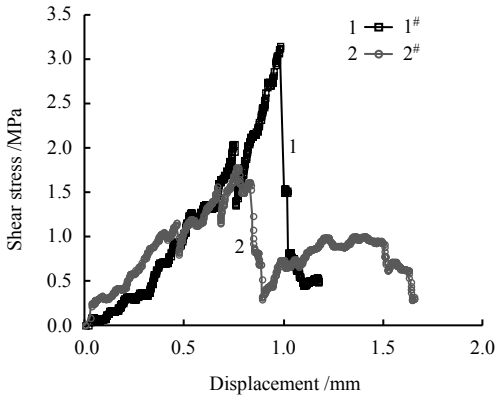

(a) Planar type

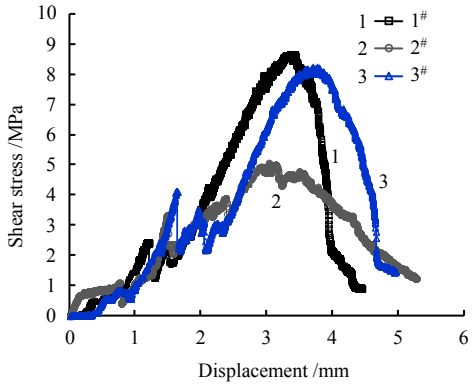

(b) Rectangle type

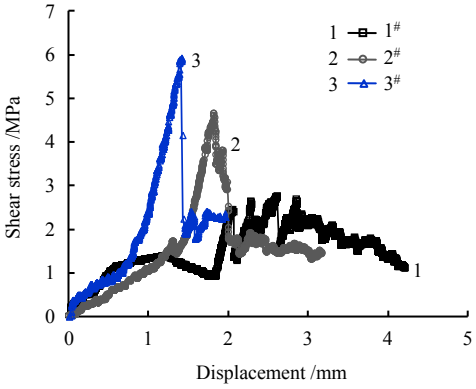

(c) Sine type

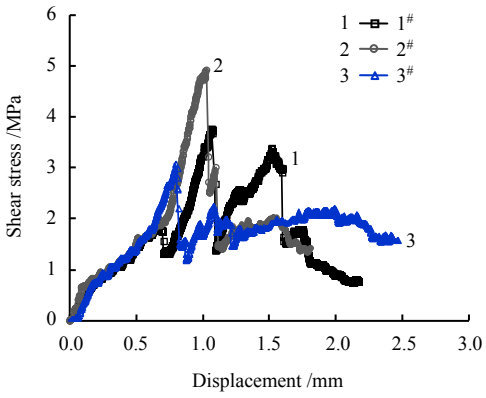

(d) Triangle type

Fig.13 Shear stress-displacement curves of varied joint models

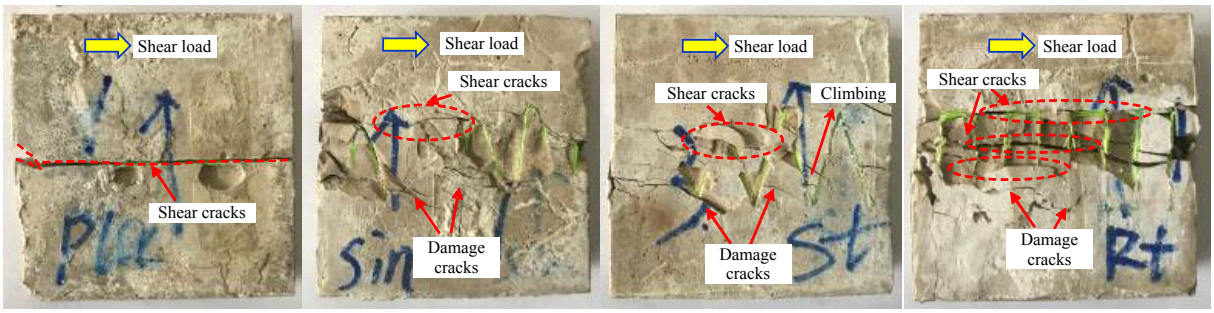

(a) Planar type (b) Sine type (c) Triangular type (d) Rectangular type

Fig.14 Shear failure modes of varied jointed rock specimens

The failure modes of jointed models with varied geometric types are shown in Fig.14. For the planar joint model, the shear failure occurs along the joint plane and the rock matrix has basically no shear failure, which is consistent with prediction. The failure mode of sinusoidal type is relatively complex. There are two macro shear cracks along the peak positions of joints. Simultaneously many shear and damage cracks appear along both the shear direction and joint traces direction. For the triangular joints, the failure mode is simpler compared with the sinusoidal type due to the linear joint surface. The failure mode is manifested mainly by initiation and propagation of shear cracks along the shear direction. Shear climbing phenomenon is found on the surface of some joint traces and the shear strength is relatively lower than that of the sinusoidal type. According to the shear stress-displacement curve in Fig.13, the rectangular joint model achieves the highest average shear strength, and its shear failure mode is also very complicated. Along the shear direction, there are at least three groups of shear cracks. Meanwhile, the rock specimen has undergone significant shear failure, and the energy required for shear fracture is relatively high. Meanwhile, significant shear failure of the rock matrix occurred along the surface of the joints. Due to the rectangular joints, the rock matrix needs to be fully fractured during the shear failure process. It is also one of the important reasons for the highest shear strength of rectangular joint models.

4.2 Fracture patterns of specimens with joints netwroks

Rock mass often contains a large number of randomly distributed discontinuities. Until recently, few experimental studies on the shear behavious of complex fractured rock masses have been reported. Many numerical researches have been performed on linear discrete fractures network (DFN) models. However, studies considering complex geometric joints is very few. Thus on the basis of our previous study [38], we prepared a linear DFN model and a rough discrete fractures network (RDFN) model, and conducted direct shear tests on the complex fracture network models. The RDFN model is an improved DFN model according to Wang et al.[39]. The main improvement is to take into account the random spatial distribution of fractures network and its own geometric complexity. Fig.15 shows the results of the shear test from the established DFN and RDFN models. Among them, the RDFN model takes into account the sine-shaped geometric distribution of joints[39].

According to mentioned preparation approach, the sulphoaluminate fast harden cement is used to make both jointed specimens (including DFN and RDFN models) and solid specimens. Fig.15(a) shows the typical shear stress-displacement curves of different types of specimens. Figs.15(b) and 15(c) show the shear failure modes of the DFN model and the RDFN model. It is found that the failure mode of solid specimens exhibit typical brittle shear failure. The failure modes of DFN model and RDFN model are relatively complicated, in which the main shear fracture surface fluctuates along the shear direction. The experimental failure mode is consistent with the numerical failure mode obtained in literature [38] using particle flow code. According to the typical shear stress-shear displacement curve, the slope of the solid specimen at the shear elastic stage is significantly higher than the joint model. The sudden drop in stress and low residual strength indicate that the solid specimen exhibits brittle shear property. The elastic stage slopes of DFN and RDFN joint models are close, indicating that the shear modulus is close. The peak shear strength of the RDFN model is higher than that of the DFN model when considering the rough characteristics of joints. The joint models show shear ductility at the post-peak stage, and the residual shear strength of the RDFN is higher than the DFN model.

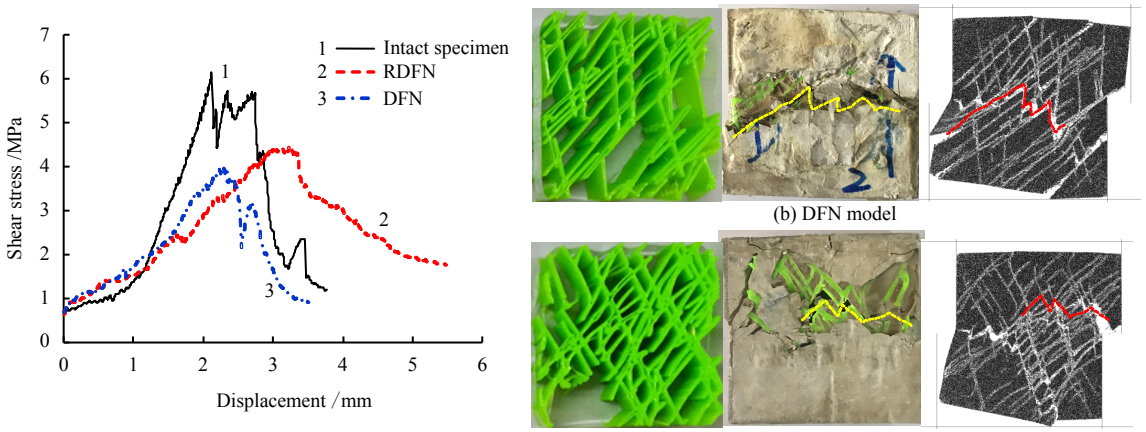

(a) Shear stress-displacement curves

(c) RDFN model

Fig.15 Shear properties of different fractured rock models

5 Conclusions

(1) This paper introduces an approach to develop joint models under complex geometric conditions using 3D printing technology. It has initially achieved the preparation of complex fractures digital models to physical models. It can efficiently and repeatably make complex joint samples with the same geometry. The work can provide a reliable physical model for the shear behaviours analysis of jointed rock mass.

(2) The shear strength of joint specimens under different JRC conditions is significantly different. As the JRC value increases, the fluctuation amplitude of joint surface generally increases, reaching the maximum when the JRC is 14 to 16. Correlation could be found between the joint amplitude and the peak shear strength. The peak shear displacement decreases with increasing fluctuation amplitude.

(3) The shear strengths of joint models with different geometric shapes are significantly different. Among them, the planar type has the lowest shear strength and the rectangular type has the highest. The shear capacities of the sinusoidal and triangular specimens are similar. The shear failure of the flat joint model occurs along the joint plane. A large number of cracks occur in all directions in the sinusoidal joint model along both the shear direction and joint traces. The fractures of the triangular joint model initiate and propagate mainly along the shear direction, while the failure mode is simpler than that of the sine type, and its shear strength is lower than that of the sine type. The rectangular joint model has some obvious shear crack coalescence along the shear direction, and many matrix rock failures occur along the joint surface, with achieving the highest shear strength .

(4) The shear strength of rock masses with complex fractures is lower than that of solid rock models. The shear strength of RDFN model considering joint roughness is higher than that of linear DFN model, indicating that the shear strength of fractured rock increases after considering the geometric roughness of joints. The failure mode of solid specimens is typical brittle shear failure, and the failure modes of DFN model and RDFN model are relatively complicated. The main shear fracture surface fluctuates along the shear direction, and the fracture surface consists of multiple joint surfaces including intersection points and joint surfaces.

References

[1] XIA Cai-chu, SUN Zong-qi. Engineering rock mass joints mechanics[M]. Shanghai: Tongji University Press, 2002: 1-5.

[2] ZHOU Hui, MENG Fan-zhen, ZHANG Chuan-qing, et al. Chinese Journal of Rock Mechanics and Engineering, 2015, 34(9): 1729-1738.

[3] DOUG S, WOLTER A. A critical review of rock slope failure mechanisms: the importance of structural geology[J]. Journal of Structural Geology, 2015, 74: 1-23.

[4] GOODMAN R E. Methods of geological engineering in discontinuous rocks[M]. New York: West Publishing Company, 1976: 472-490.

[5] BARTON N. Review of a new shear strength criterion for rock joints[J]. Engineering Geology, 1973, 7(4): 287-332.

[6] BARTON N, CHOUBEY V. The shear strength of rock joints in theory and practice[J]. Rock Mechanics, 1977, 10(1-2): 1-54.

[7] International Society for Rock Mechanics. Suggested methods for the quantitative description of discontinuities in rock masses[J]. International Journal of Rock

Mechanics and Mining Sciences, 1978, 15(6): 319-368.

[8] BANDIS S C, LUMSDEN A C, BARTON N R. Fundamentals of rock joint deformation[J]. International Journal of Rock Mechanics and Mining Sciences & Geomechanics Abstracts, 1983, 20(6): 249-268.

[9] LEE H S, PARK Y J, CHO T F. Influence of asperity degradation on the mechanical behavior of rough rock joints under cyclic shear loading[J]. International Journal of Rock Mechanics and Mining Sciences, 2001, 38(7): 967-980.

[10] HOMAND F, BELEM T, SOULEY M. Friction and degradation of rock joint surfaces under shear loads[J]. International Journal for Numerical and Analytical Methods in Geomechanics, 2001, 25(10): 973-999.

[11] JAFARI M K, PELLET F, BOULON M. Experimental study of mechanical behaviour of rock joints under cyclic loading[J]. Rock Mechanics and Rock Engineering, 2004, 37(1): 3-23.

[12] JIANG Y J, LI B, TANABASHI Y. Estimating the relation between surface roughness and mechanical properties of rock joints[J]. International Journal of Rock Mechanics and Mining Sciences, 2006, 43(6): 837-846.

[13] JIANG Yu-jing, WANG Gang, LI Bo, et al. Chinese Journal of Rock Mechanics and Engineering, 2007, 26(11): 2253-2259.

[14] SINGH H K, BASU A. Shear behaviors of ‘real’ natural un-matching joints of granite with equivalent joint roughness coefficients[J]. Engineering Geology, 2016, 211: 120-134.

[15] SINGH H K, BASU A. Evaluation of existing criteria in estimating shear strength of natural rock discontinuities[J]. Engineering Geology, 2018, 232: 171-181.

[16] ZHAO Z, PENG H, WU W, et al. Characteristics of shear-induced asperity degradation of rock fractures and implications for solute retardation[J]. International Journal of Rock Mechanics and Mining Sciences, 2018, 105: 53-61.

[17] NIKTABAR S M M, RAO K S, SHRIVASTAVA A K. Effect of rock joint roughness on its cyclic shear behavior[J]. Journal of Rock Mechanics and Geotechnical Engineering, 2017, 9(6): 1071-1084.

[18] CHENG Y, YANG W, HE D. Influence of sample size on the shear strength of structural plane[J]. Geotechnical and Geological Engineering, 2018: 1-8.

[19] TIAN Y, LIU Q, MA H, et al. New peak shear strength model for cement filled rock joints[J]. Engineering Geology, 2018, 233: 269−280.

[20] ZHOU Hui, CHENG Guang-tan, ZHU Yong, et al. Rock and Soil Mechanics, 2019, 40(3): 852-860.

[21] LU B H, LI D C, TIAN X Y. Development trends in additive manufacturing and 3D printing[J]. Engineering, 2015, 1(1): 85-89.

[22] JU Yang, XIE He-ping, ZHENG Ze-min, et al. Chinese Science Bulletin, 2014, 59(32): 3019-3119.

[23] FERESHTENEJAD S, SONG J J. Fundamental study on applicability of powder-based 3D printer for physical modeling in rock mechanics[J]. Rock Mechanics and Rock Engineering, 2016, 49(6): 2065-2074.

[24] JIANG Q, FENG X, GONG Y, et al. Reverse modelling of natural rock joints using 3D scanning and 3D printing[J]. Computers and Geotechnics, 2016, 73: 210-220.

[25] LIU P, JU Y, RANJITH PG, et al. Visual representation and characterization of three-dimensional hydrofracturing cracks within heterogeneous rock through 3D printing and transparent models[J]. International Journal of Coal Science and Technology, 2016, 3(3): 284-294.

[26] TIAN W, HAN N. Preliminary research on mechanical properties of 3D printed rock structures[J]. Geotechnical Testing Journal, 2017, 40(3): 483-493.

[27] JIANG Quan, SONG Lei-bo. Chinese Journal of Rock Mechanics and Engineering, 2018, 37(1): 23-37.

[28] XIE He-ping, GAO Feng, JU Yang. Chinese Journal of Rock Mechanics and Engineering, 2015, 34(11): 2161-2178.

[29] JU Y, XIE H P, ZHENG Z M, et al. Visualization of the complex structure and stress field inside rock by means of 3D printing technology[J]. Chinese Science Bulletin, 2014, 59(36): 5354-5365.

[30] XIONG Zu-qiang, JIANG Quan, GONG Yan-hua, et al. Rock and Soil Mechanics, 2015, 36(6): 1557-1565.

[31] TIAN Wei, PEI Zhi-ru, HAN Nü. Rock and Soil Mechanics, 2017, 38(8): 2297-2305.

[32] WANG Pei-tao, LIU Yu, ZHANG Liang, et al. Chinese Journal of Rock Mechanics and Engineering, 2018, 37(2): 364-373.

[33] ZHU J B, ZHOU T, LIAO Z Y, et al. Replication of internal defects and investigation of mechanical and fracture behaviour of rock using 3D printing and 3D numerical methods in combination with X-ray computerized tomography[J]. International Journal of Rock Mechanics and Mining Sciences, 2018, 106: 198-212.

[34] SONG L B, JIANG Q, SHI Y E, et al. Feasibility investigation of 3D printing technology for geotechnical

physical models: study of tunnels[J]. Rock Mechanics and Rock Engineering, 2018, 51(8): 2617-2637.

[35] KONG L, OSTADHASSAN M, LI C, et al. Pore characterization of 3D-printed gypsum rocks: a comprehensive approach[J]. Journal of Materials Science, 2018, 53(7): 5063-5078.

[36] KONG L, OSTADHASSAN M, LI C, et al. Can 3D printed gypsum samples replicate natural rocks? An experimental study[J]. Rock Mechanics and Rock Engineering, 2018, 51(10): 3061-3074.

[37] ZHOU Hui, CHENG Guang-tan, ZHU Yong, et al. Rock and Soil Mechanics, 2019, 40(1): 118-126.

[38] WANG Pei-tao, REN Fen-hua, CAI Mei-feng. Journal of China Coal Society, 2018, 43(4): 976-983.

[39] WANG Pei-tao, REN Fen-hua, TAN Wen-hui, et al. Rock and Soil Mechanics, 2017, 38(Suppl.1): 76-84.